Wear 306 (2013) 248–253

Contents lists available at ScienceDirect

Wear

journal homepage: www.elsevier.com/locate/wear

Potential of graphene layer controlling nano-wear during C_{60} intrusion by molecular dynamics simulation

Qi Zhang, Dongfeng Diao*

Key Laboratory of Education Ministry for Modern Design and Rotor-Bearing System, School of Mechanical Engineering, Xi'an Jiaotong University, Xi'an 710049, China

ARTICLE INFO

Article history:
Received 26 April 2012
Received in revised form
9 September 2012
Accepted 17 September 2012
Available online 16 October 2012

Keywords:
Graphene
C_{60}
Nano-wear
No-wear
Molecular dynamics simulation
Intrusion

ABSTRACT

The intrusion process of a C_{60} (the smallest ball in nature) into a sliding contact space was simulated using the Molecular Dynamics approach. The contact space consisted of upper and lower Si substrates layered by graphene with an included angle changing from 20° to 90°, and C_{60} just contacted with both the upper and lower substrates. A constant horizontal speed 3 nm/ps was applied to the lower substrate, and the process of C_{60} breaking through the contact space was observed. During this process, the nano-wear of the substrate was evaluated by the number of dropped atoms from the substrates. The results showed the number of dropped atoms from the upper Si substrate was dependent on the initial included angle and the graphene layered positions. The potential that graphene can control nano-wear and realize no-wear of the surface was revealed, also the potential that graphene can control C_{60} intrusion into the sliding contact space was found.

1. Introduction

Since graphene was prepared experimentally, it has become a glowing material in scientific field [1–3]. Various studies focused on its prominent properties such as superior electronic properties [4,5], outstanding mechanical properties [6,7], and extremely high thermal conductivity [8,9]. Graphene was found to be effective solid lubricant additives [10,11]. The friction force on the graphene layer presented a periodic variation of stick-slip [12]. However, few studies pay attention to that graphene can prevent nano-wear of the contact surfaces in motion.

Nano-wear of micro surfaces leads to significant impact on the performances of nano devices, and many researchers make great efforts to find various materials controlling nano-wear. Khurshudov et al. [13] studied nano-wear of the atomic force microscopy diamond tip when scratching a Si substrate. The nano-wear characteristics of alkanethiol self-assembled monolayer were studied by Sung and Kim [14] using molecular dynamics simulation. However, little information from the previous studies was found to realize no-wear of the surface. Graphene, on the other hand, is expected to control nano-wear, since the intrinsic strength is predicted to exceed that of any other material [3].

C_{60}, a stable cluster as the smallest ball in nature is an ideal material to study the interactions of nanopaticles with surfaces or the nanoparticle intrusion into a sliding space. The ultra low friction between C_{60} and graphite was studied in the model where the C_{60} balls were inserted between two parallel graphite sheets [15,16]. He et al. [17] observed the generation of dynamics ripples in graphene stroked by C_{60}. The impact mechanics of C_{60} collisions on various surfaces were investigated, and graphene could be formed from C_{60} molecular fragments using surface collisions [18–20]. In our previous work, we have simulated an intrusion process of C_{60} ball into the Si sliding contact space with an included angle from 20° to 90°, which is simplified from the cleaning system of laser printer, and found nano-wear of Si substrate by atom loss [21]. In this paper, we explored the potential of graphene layer in controlling nano-wear of contact space protected by graphene. For this purpose, we studied the processes of a C_{60} sliding against the contact surfaces using molecular dynamics (MD) approach. Furthermore, this study also explored an interesting scientific problem how C_{60} passed through a sliding contact space and how the graphene layer controlled the passing.

2. Methods

Fig. 1 shows the MD model for the simulation. The material of lower and upper substrates was Si (100) with the size of $A_1 \times B_1 \times C_1 = 10.860\ \text{nm} \times 4.340\ \text{nm} \times 1.629\ \text{nm}$ (containing 4145 atoms) and $A_2 \times B_2 \times C_2 = 4.887\ \text{nm} \times 2.172\ \text{nm} \times 1.086\ \text{nm}$ (containing 716 atoms), respectively.

* Corresponding author. Tel./fax: +86 29 82669151.
E-mail address: dfdiao@mail.xjtu.edu.cn (D. Diao).

0043-1648/$ - see front matter © 2012 Elsevier B.V. All rights reserved.
http://dx.doi.org/10.1016/j.wear.2012.09.003

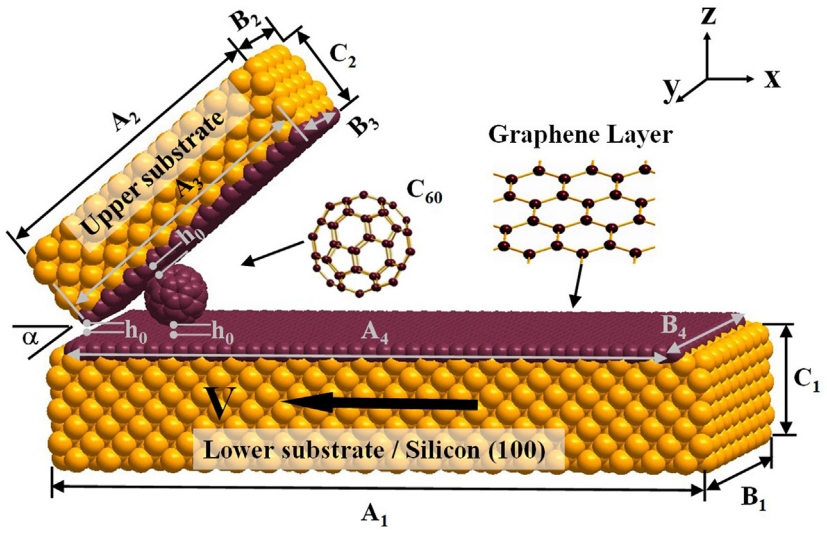

Fig. 1. (a) MD simulation model for C_{60} ball intrusion into a sliding space with graphene layers.

Graphene was layered on different positions to form three models. In the first model (M1), the upper substrate was layered by graphene, and the size of the graphene layer was $A_3 \times B_3 = 4.797\ \text{nm} \times 2.130\ \text{nm}$ (containing 420 atoms). In the second model (M2), the lower substrate was layered by graphene, and the size of the graphene layer was $A_4 \times B_4 = 10.209\ \text{nm} \times 4.331\ \text{nm}$ (containing 1746 atoms). In the third model (M3), both the substrates were layered by graphene. The lower substrate was horizontal, and the upper substrate was inclined forming an included angle α.

In the simulation, Tersoff potential as a popular multibody interaction potential was applied to calculate the interactions among Si atoms and C atoms [22,23]. The total Tersoff energy E can be expressed as in Eq. (1)

$$E = \sum_i E_i = \frac{1}{2}\sum_{i \neq j} V_{ij} \tag{1}$$

where, j and k are the neighboring atoms of atom i. V_{ij} is the bond energy, the function of the repulsive pair potential f_R and the attractive pair potential f_A, and has the following form

$$V_{ij} = f_C(r_{ij})[f_R(r_{ij}) + b_{ij} f_A(r_{ij})] \tag{2}$$

where the bond lengths of atoms i–j and i–k are r_{ij} and r_{ik}, and

$$f_R(r_{ij}) = A_{ij}\exp\left(-\lambda_{ij} r_{ij}\right), \quad f_A(r_{ij}) = -B_{ij}\exp\left(-\mu_{ij} r_{ij}\right);$$

$$f_C(r_{ij}) = \begin{cases} 1, r_{ij} < R_{ij}, \\ 0.5 + 0.5\cos\,\pi[(r_{ij} - R_{ij})/(S_{ij} - R_{ij})], R_{ij} < r_{ij} < S_{ij}, \\ 0, r_{ij} > S_{ij}; \end{cases}$$

$$b_{ij} = \chi_{ij}\left(1 + \beta_i^{n_i}\zeta_{ij}^{n_i}\right)^{-1/2n_i},$$

$$\zeta_{ij} = \sum_{k \neq i,j} f_C(r_{ik}) g(\theta_{ijk});$$

$$g(\theta_{ijk}) = 1 + c_i^2/d_i^2 - c_i^2/[d_i^2 + (h_i - \cos\theta_{ijk})^2];$$

$$\lambda_{ij} = (\lambda_i + \lambda_j)/2,\ \mu_{ij} = \left(\mu_i + \mu_j\right)/2,\ A_{ij} = (A_i A_j)^{1/2};$$

$$B_{ij} = (B_i B_j)^{1/2},\ R_{ij} = (R_i R_j)^{1/2},\ S_{ij} = (S_i S_j)^{1/2}.$$

the parameters such as A, B, R, S, λ, χ and μ, are listed in Table 1. With Eqs. (1) and (2), the interaction forces among Si atoms and C atoms can be obtained by calculating the gradient of total Tersoff energy E [24,25].

Free boundary conditions were applied in the simulation. One bottom layer and one outermost layer around the lower substrate were fixed. Also the two rightmost layers of the upper substrate were fixed, and the rest atoms were free as thermostat atoms at 300 K by rescaling their velocities.

Table 1
Parameters in Tersoff potential for C and Si [24].

Material	C	Si
A (eV)	1.3936×10^3	1.8308×10^3
B (eV)	3.4670×10^2	4.7118×10^2
λ (nm^{-1})	0.34879	0.24799
μ (nm^{-1})	0.22119	0.17322
β	1.5724×10^{-7}	1.1000×10^{-6}
n	7.2751×10^{-1}	7.8734×10^{-1}
c	3.8049×10^4	1.0039×10^5
d	4.384×10^0	1.6217×10^1
h	-5.7058×10^{-1}	-5.9825×10^{-1}
R (nm)	0.18	0.27
S (nm)	0.21	0.30
$\chi_{C-C} = 1.0$	$\chi_{Si-Si} = 1.0$	$\chi_{C-Si} = 0.9776$

The initial contact condition of C_{60} with the substrates was shown in Fig. 1 where the initial distance h_0 between the upper and the lower substrate at the tip is decided as a cutoff distance (the cutoff distance is 0.25 nm for Si–C, 0.21 nm for C–C, and 0.30 nm for Si–Si), the initial distance between C_{60} and the substrates is also the cutoff distance. According to Eq. (2), if h_0 is larger than the cutoff distance, there is no interaction force among bodies. In this way, it can balance the system and save the simulation time, and initially there is no contact atom at the interface between the substrates. In order to clarify the influence of the initial included angle on nano-wear of the substrate surfaces, α was changed from 20° to 90° by every 2°.

A constant velocity of 3 nm/ps in the negative x-direction was imposed on the lower substrate. The simulation ran for 3000 time steps and each time step was 0.001 ps, therefore the total sliding distance of the lower substrate is 9 nm which was long enough to observe the intrusion process. The system ran without external force because when the rightmost of upper substrate was fixed, the upper substrate will give C_{60} a counterforce during the intrusion, so we do not take into account the load and pressure on the upper substrate.

In this study, nano-wear of contact surface was evaluated by the number of dropped atoms. The dropped atom was defined as the Si atom which moved from the substrate surface for a distance longer than the cutoff distance (0.27 nm).

3. Results

Fig. 2 shows the sliding processes of the systems without and with graphene layer when the initial included angle was 40°. As shown in Fig. 2(a), when the substrate was not layered graphene, C_{60} was moving with the lower substrate along the negative x-direction, pressing the tip of the upper substrate to bend. When the simulation ran for 1200 time steps, the upper substrate was lifted and C_{60} was just between the two substrates. Afterward, the deformation of the upper substrate recovered when C_{60} passed the contact space. During the sliding process, it was obvious that some Si atoms of the upper substrate were permanently displaced as dropped atoms because of the interactions among the substrates and C_{60}. When graphene was layered on the upper substrate (M1, see Fig. 2(b)), the upper substrate bended a little during the sliding process, and only the Si atoms on the bottom of the upper substrate were pulled off. The wear of the upper substrate is dependent not only on the intrusion of C_{60}, but also the interactions between the two substrates. In this system, less leftmost upper Si atoms directly faced to the lower substrate when the angle was smaller, which means the distance between leftmost upper Si atoms and the lower surface was longer, leading to smaller interaction between the two substrates. As a result, less upper substrate atoms were pulled off when the angle is small.

However, in M2 and M3 (Fig. 2(c) and (d)), the results were desirable that no atom loss occurred on the upper substrate overall the sliding processes and the upper substrate just bended slightly. This indicated that when graphene was layered on the lower substrate or both the substrates, no-wear of the upper substrate can be realized.

During the sliding process, the upper substrate was acted by the attractive and repulsive forces as well as the friction force from the lower substrate and C_{60}. Fig. 2(e) shows the variation of the x-direction forces of the upper substrate with each time step in M1, M2 and M3 when α was 40°. The forces of the upper substrate changed irregularly with the increasing time steps. However, it was observed that the forces on the upper substrate were much larger in M1 than those in M2 and M3. Meanwhile, similar trends were found in the z-direction forces. As a result, the bonds in the upper substrate were more likely to be broken by the

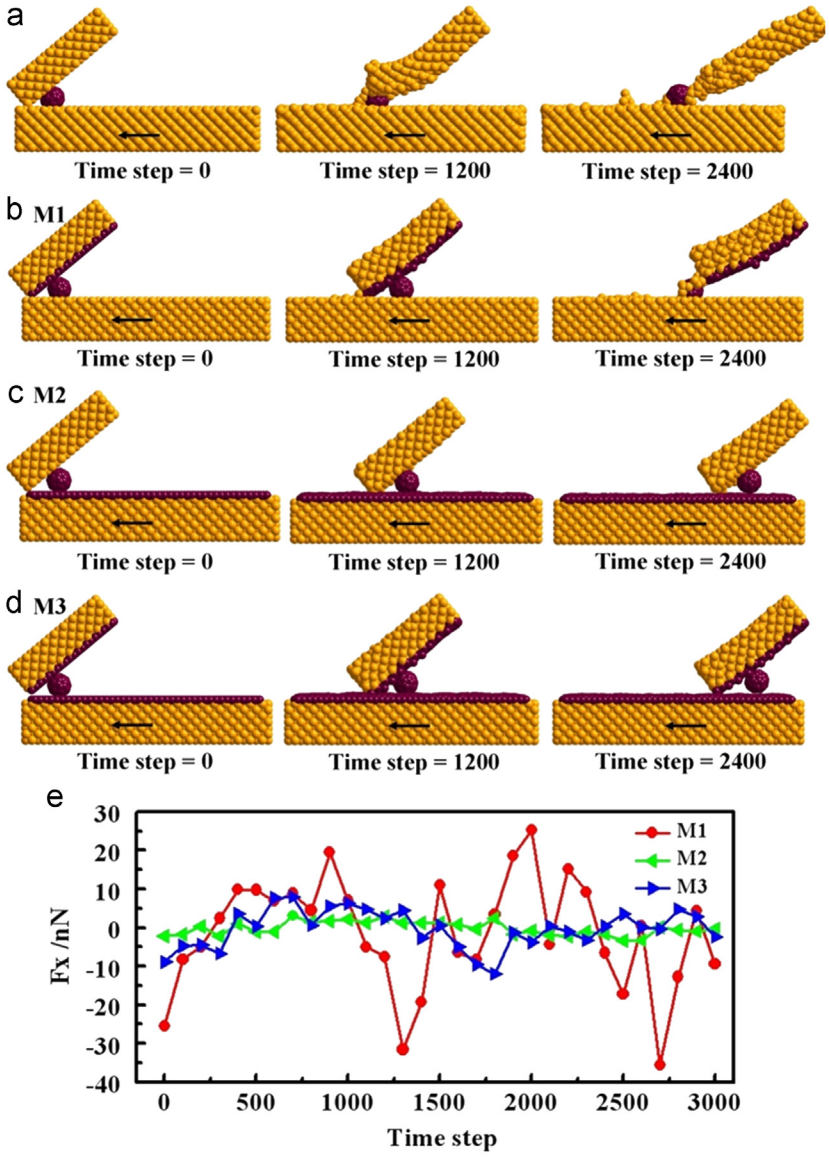

Fig. 2. Simulation results with the initial included angle α of 40°. (a) The snapshots of sliding process when the substrates without graphene layer. (b)–(d) The movement snapshots of M1, M2 and M3, respectively. (e) The x-direction forces of the upper substrate changing with the increasing time steps in M1 (red circle), M2 (green triangle) and M3 (blue triangle). (For interpretation of the references to color in this figure legend, the reader is referred to the web version of this article.)

forces with larger fluctuations in M1, producing the dropped atoms which lead to nano-wear of the upper substrate.

Fig. 3 shows the simulation results of the systems running for 2400 time steps at different initial included angles (40°, 80° and 90°). In M1, the initial included angle was an important factor (Fig. 3(a)). When the initial angle was 40°, only a few atoms of the upper substrate were pulled off. More atoms dropped and stuck to C_{60} and the lower substrate when α was 80°, and the bottom of the upper substrate was stretched by the moving lower substrate. Additionally, because the two rightmost layers of the upper substrate were fixed, the included angle turned to be much smaller than 80° at the end of the simulation. When α was 90°, nano-wear of the upper substrate became even more serious, also the included angle became smaller. Fig. 4 shows the simulation results of C_{60} intrusion process at the initial included angle of 90°. C_{60} was moving with the lower substrate, the bottom of the upper substrate was close to lower surface and these atoms were attached during sliding. With the moving of the lower substrate, the bottom of the upper substrate was pulled by the lower substrate leading to smaller included angle. In Fig. 4(f), it is clearly observed that a large number of atoms near the contact area move away from the upper substrate. Further sliding lead to the bonds broken in the upper substrate, and finally a number of atoms of the upper substrate were pulled down and stuck to the lower substrate (Fig. 4(h)). C_{60} cannot intrude into the sliding contact space and be surrounded by the sticking atoms from the upper substrate. Therefore, when the upper substrate was layered by graphene, nano-wear became more and more serious with the increasing α. However, when graphene was layered on the lower substrate, no dropped atom was pulled off from the upper substrate regardless of α. The same phenomenon was observed when graphene was layered on both substrates.

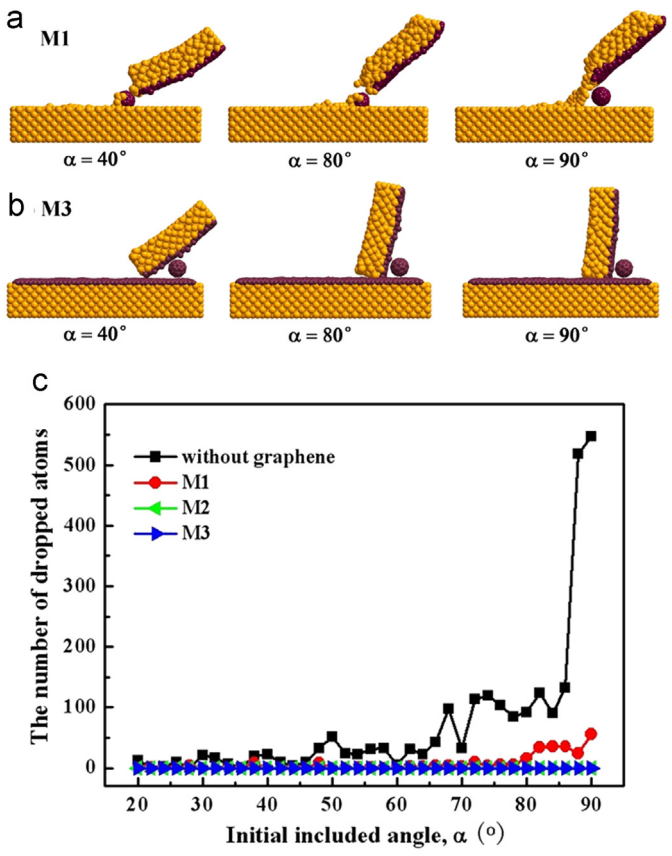

Fig. 3. The results after the simulations running for 2400 steps. (a) and (b) are the simulation snapshots of M1 and M3 at different initial included angles α (40°, 80° and 90°, respectively). The simulation results of M2 were not shown because they were similar to the results of M3. (c) shows the number of dropped atoms with variation of initial included angles for the system without graphene layer (black square), M1 (red circle), M2 (green triangle) and M3 (blue triangle). (For interpretation of the references to color in this figure legend, the reader is referred to the web version of this article.)

The numbers of dropped atoms with different initial included angles are summarized in Fig. 3(c). In the system without graphene layer, the variation of the dropped atoms with the initial included angles appeared in three different tendencies. When α was less than 70°, the number of dropped atoms was no more than 50, and it increased slowly with the increasing of initial included angle. When the initial angle was between 70° and 85°, there were about 100 dropped atoms. When the initial angle was more than 85°, the number of dropped atoms was sharply up to about 550. However, in M1, it was obvious that the number of dropped atoms decreased a lot. When α was less than 80°, there was no dropped atom in most cases. While α was larger than 80°, the number of dropped atoms increased to 56, which was much less than that in the system without graphene layer. More significantly, in M2 and M3, the numbers of dropped atoms were always zero and had no concern with the initial included angle. Accordingly, graphene layer possesses a great potential for controlling the surface nano-wear and realizing no-wear during sliding.

Another potential of graphene layer was also found out that it can defend C_{60} intruding into the contact space. From the results of M1 (shown in Fig. 3(a)), C_{60} could intrude into the contact space if α was 40° or 80°. As α increased to 90°, C_{60} was stopped by the dropped atoms and could not intrude into the contact space. However, when the lower substrate was layered by graphene or both of the substrates were layered by graphene, C_{60} was always confined to the right side of the contact space whatever the initial included angle was (shown in Fig. 3(b)). This means that graphene layer has the potential for defending C_{60} intrusion without nano-wear. It is presumed that, under the same condition, a larger nanoparticle cannot intrude into the contact space if C_{60} (the smallest ball in nature) cannot break through. This is important for nanoparticle cleaning or nano device sealing. Especially in space where fullerenes are abundant [26,27], graphene as the protective layer for space-based devices will show its glory.

Taken together, a critical initial included angle α_c was found to be 85° in the system without graphene layer. When α was larger than α_c, nano-wear of the upper substrate became more severe but C_{60} could not intrude into the contact space. There also existed a α_c of 80° in M1. On the contrary, in M2 and M3, no matter what initial included angle was, no-wear of the upper substrate was realized and the intrusion of C_{60} was stopped by graphene layer.

4. Discussions

In M1, where the upper substrate was layered by graphene, nano-wear of the upper substrate was much more serious compared to the results in M2 and M3. That was because the Si atoms in the leftmost layer of the upper substrate were not protected by graphene layer, and these atoms faced to the Si atoms in the lower substrate surface. During the moving of the system, the Si atoms which exposed at the surface were not stable and would shift to various directions when the interactions among the substrates and C_{60} forced on these atoms [28]. Then the original Si–Si bonds were broken, and Si atoms of the upper substrate would stick to C_{60} or the lower Si surface. In order to protect the leftmost of the upper substrate, the M1 was improved in which graphene was also layered on the leftmost of the upper substrate. Fig. 5 shows the simulation results when α is 40°. In order to distinguish wear of the upper

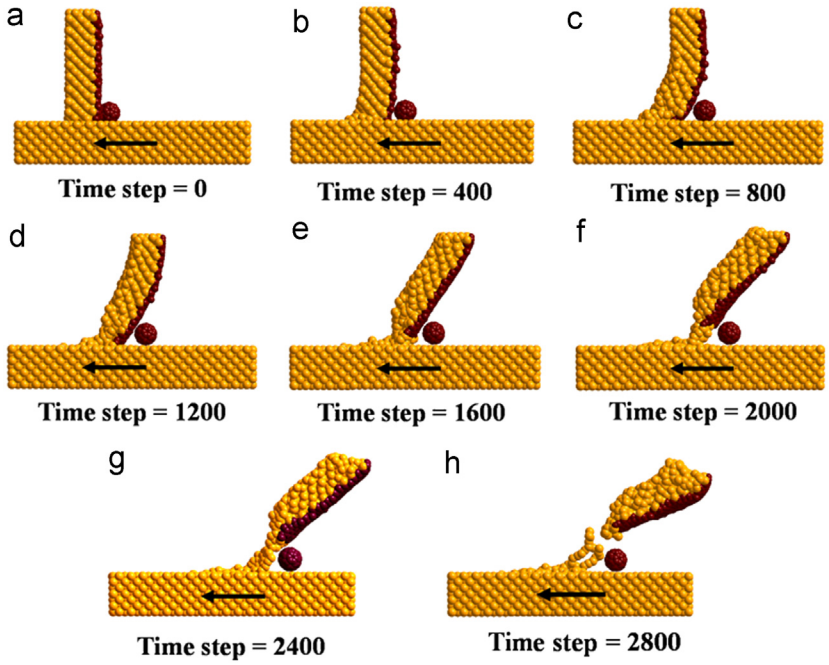

Fig. 4. The snapshots of sliding process in M1 (the upper substrates is layered by graphene) when the initial included angle is 90°.

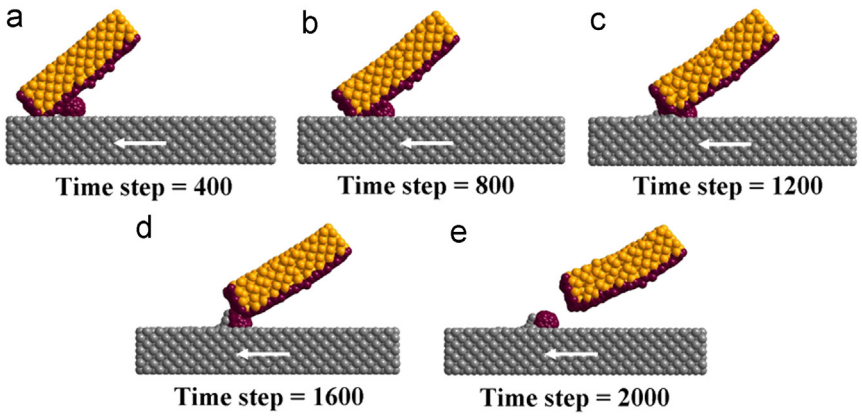

Fig. 5. The simulation results of the improved M1 in which the leftmost of the upper substrate was layered by graphene as the initial included angle α was 40°.

substrate from that of the lower substrate, the atoms in the lower substrate were shown in gray color. C_{60} sunk into the lower substrate and some Si atoms of the lower substrate absorbed to C_{60}. But no atom of the upper substrate was pulled off. It was inferred that if graphene completely surrounded one of the contact surfaces, no-wear of the upper substrate could be realized.

In order to learn about the effect of other initial conditions on the wear of the upper substrate, we compared the calculation results with different velocities and temperature control methods. In M1 (the system where the upper substrate is layered by graphene), the lower substrate was forced by 30 m/s (0.03 nm/ps), and during the sliding process, only 2 dropped atoms from the upper substrate were produced when the initial included angle was 40°. Compared to the result when the velocity was 3 nm/ps, the effect of speed on the wear of the upper substrate was not great, and the velocity 3 nm/ps can save a lot of calculation time. Then in this model, we changed the temperature control method: only fixed one bottom layer and one outermost layer around the lower substrate as well as the two rightmost layers of the upper substrate at 300 K. The number of dropped atoms from the upper substrate was also zero, the same as the result with all the atoms fixed at 300 K.

5. Conclusions

Nano-wear controlled by graphene layer was studied using molecular dynamics simulation, in which two potentials of graphene layer were discovered. First, no-wear can be realized through layering graphene on the substrate surfaces. Second, the graphene layer can be a promising material to defend the nanoparticle such as C_{60} intrusion into a contact space. These findings provide deep insights in understanding the self-protection of graphene-based materials and will prospect for wider graphene applications in physical, mechanical, electromechanical, and biomedical fields.

Acknowledgment

The authors sincerely thank the National Nature Science Foundation of China under Grant Nos. of 90923027 and 51175405, the Ricoh Printing System in Japan for cooperation.

References

[1] K.S. Novoselov, A.K. Geim, S.V. Morozov, D. Jiang, Y. Zhang, S.V. Dubonos, I.V. Grigorieva1, A.A. Firsov, Electric field effect in atomically thin carbon films, Science 306 (2004) 666–669.

[2] C. Lee, X. Wei, W.K. Jeffrey, H. James, Measurement of the elastic properties and intrinsic strength of monolayer graphene, Science 321 (2008) 385–388.

[3] Q. Zhao, M.B. Nardelli, J. Bernholc, Ultimate strength of carbon nanotubes: A theoretical study, Physical Review B 65 (2002) 144105–144106.

[4] K.S. Novoselov, A.K. Geim, S.V. Morozov, D. Jiang, M.I. Katsnelson, I.V. Grigorieva, S.V. Dubonos, A.A. Firsov, Two-dimensional gas of massless Dirac fermions in graphene, Nature (London) 438 (2005) 197–200.

[5] Y. Zhang, J.P. Small, W.V. Pontius, P. Kim, Fabrication and electric-field-dependent transport measurements of mesoscopic graphite devices, Applied Physics Letters 86 (2005) 073104–073106.

[6] Y.Y. Zhang, C.M. Wang, Y. Cheng, Y. Xiang, Mechanical properties of bilayer graphene sheets coupled by sp3 bonding, Carbon 49 (2011) 4511–4517.

[7] J.W. Suk, R.D. Piner, J. An, R.S. Ruoff, Mechanical properties of monolayer graphene oxide, ACS Nano 4 (2010) 6557–6564.

[8] S. Ghosh, I. Calizo, D. Teweldebrhan, E.P. Pokatilov, D.L. Nika, A.A. Balandin, W. Bao, F. Miao, C.N. Lau, Extremely high thermal conductivity of graphene: prospects for thermal management applications in nanoelectronic circuits, Applied Physics Letters 92 (2008) 151911–151913.

[9] R. Prasher, Graphene spreads the heat, Science 328 (2010) 185–186.

[10] J. Lin, L. Wang, G. Chen, Modification of graphene platelets and their tribological properties as a lubricant additive, Tribology Letters 41 (2011) 209–215.

[11] L. Wang, L. Zhang, M. Tian, Effect of expanded graphite (EG) dispersion on the mechanical and tribological properties of nitrile rubber/EG composites, Wear 276–277 (2012) 85–93.

[12] L. Xu, T. Ma, Y. Hu, H. Wang, Molecular dynamics simulation of the interlayer sliding behavior in few-layer graphene, Carbon 50 (2012) 1025–1032.

[13] A.G. Khurshudov, K. Kato, H. Koide, Wear of the AFM diamond tip sliding against silicon, Wear 203–204 (1997) 22–27.

[14] I.H. Sung, D.E. Kim, Molecular dynamics simulation study of the nano-wear characteristics of alkanethiol self-assembled monolayers, Applied Physics A 81 (2005) 109–114.

[15] K. Miura, S. Kamiya, N. Sasaki, C_{60} Molecular Bearings, Physical Review Letters 90 (2003) 055509–055512.

[16] S.B. Legoas, R. Giro, D.S. Galvao, Molecular dynamics simulations of C_{60} nanobearings, Chemical Physics Letters 386 (2004) 425–429.

[17] Y.Z. He, H. Li, P.C. Si, Y.F. Li, H.Q. Yu, X.Q. Zhang, F. Ding, K.M. Liew, X.F. Liu, Dynamic ripples in single layer graphene, Applied Physics Letters 98 (2011) 063101–063103.

[18] G. Galli, F. Mauri, Large scale quantum simulations: C_{60} impacts on a semiconducting surface, Physical Review Letters 73 (1994) 3471–3474.

[19] R.D. Beck, C. Warth, K. May, M.M. Kappes, Surface impact induced shattering of C_{60}. Detection of small C_m fragments by negative surface ionization, Chemical Physics Letters 257 (1996) 557–562.

[20] J. Lu, P.S.E. Yeo, C.K. Gan, P. Wu, K.P. Loh, Transforming C_{60} molecules into graphene quantum dots, Nature Nanotech 6 (2011) 247–252.

[21] P. Li, D.F. Diao, Molecular dynamics simulation of intrusion of a C_{60} molecule ball into sliding contact space, Lubrication Science 24 (2012) 1–10.

[22] L.C. Zhang, H. Tanaka, On the mechanics and physics in the nano-indentation of silicon monocrystals, JSME International Journal 42 (1999) 546–559.

[23] Y.H. Lin, T.C. Chen, P.F. Yang, S.R. Jian, Y.S. Lai, Atomic-level simulations of nanoindentation-induced phase transformation in mono-crystalline silicon, Applied Surface Science 254 (2007) 1415–1422.

[24] J. Tersoff, New empirical approach for the structure and energy of covalent systems, Physical Review B 37 (1988) 6991–7000.

[25] J. Tersoff, Modeling solid-state chemistry: interatomic potentials for multi-component systems, Physical Review B 39 (1989) 5566–5568.

[26] J. Cami, J. Bernard-Salas, E. Peeters, S.E. Malek, Detection of C_{60} and C_{70} in a young planetary nebula, Science 329 (2010) 1180–1182.

[27] P. Ehrenfreund, B.H. Foing, Fullerenes and cosmic carbon, Science 329 (2010) 1159–1160.

[28] M.T. Yin, Si-III (BC-8) crystal phase of Si and C: structural properties, phase stabilities, and phase transitions, Physical Review B 30 (1984) 1773–1776.